A Two-Wired Ultra-High Input Impedance Active Electrode

Federico Nicolás Guerrero and Enrique Mario Spinelli

***Abstract*—This paper presents a novel two-wired active electrode that achieves ultrahigh input impedance using power supply bootstrapping. The proposed circuit reduces the input capacitance of a buffer amplifier while enabling measurements using leads with only two wires, providing a low-complexity and low-cost solution for interference rejection and artifact reduction in dc-coupled dry-contact biopotential measurements. An implemented prototype shows that, even using standard operational amplifiers, an input capacitance as low as 71 fF can be obtained, maintaining a high impedance in a 0–1 kHz bandwidth, sufficient for ECG, EEG, and EMG measurements. The circuit has a simple and easily replicable implementation that requires no individual adjustment. A common mode rejection ratio (CMRR) above 103 dB at 50 Hz was achieved and the increased rejection to interference due to the potential divider effect was experimentally tested maintaining a 92-dB CMRR at 50 Hz with a 1.2-MΩ source impedance unbalance. ECG measurements were conducted to validate the active electrode against a traditional alternative, and a test with dry-contact EEG electrodes was successfully conducted. Although the proposed circuit is intended to acquire superficial electrophysiological signals using dry electrodes, it can be used for measurement from other high-impedance sources, such as micropipette electrodes.**

***Index Terms*—Active electrodes, biopotential measurements, dry-contact electrodes, power supply bootstrapping, two-wired buffer.**

I. Introduction

NON-INVASIVE biopotential measurements using dry-contact electrodes have the potential to enable or enhance a wide range of applications including chronic patient monitoring, brain-computer interfaces (BCIs), biofeedback, and even consumer devices. Dry electrodes are tailored for the patient or user comfort; they are simple to install, require no gel, which may irritate skin, and can be used for longer periods without performance loss due to electrolyte drying. However, dry electrodes have a higher impedance than the wet kind, with high variability. Impedance values range between 100 kΩ and a few MΩ, even surpassing the order of 10 MΩ during the first minutes after application [1]–[7].

Although current front-ends have a very high CMRR, unbalanced electrode impedances produce interference through the so-called "potential divider effect" [8]. The potential divider effect creates a common mode (CM) to differential mode (DM) transformation regardless of the CMRR of the system. Considering a differential measurement channel with electrode impedance unbalance ΔZ_e and CM input impedance Z_c, a common mode voltage signal v_CM produces an interference signal *at the differential input of the system* approximately equal to [8]:

$$v_\mathrm{d,i} \approx v_\mathrm{CM}\,\Delta Z_\mathrm{e}/Z_\mathrm{c} \tag{1}$$

The use of active electrodes is a well established way of countering the potential divider effect by presenting a high Z_c that reduces the magnitude of (1). However, if a system is implemented with off-the-shelf commercial components, the input impedance is limited by their input capacitance which is at best 1 pF. Considering $Z_\mathrm{c} \approx (2\pi \times 50\,\mathrm{Hz} \times 1\,\mathrm{pF})^{-1}$ and $|\Delta Z_\mathrm{e}| = 1\ \mathrm{M\Omega}$, (1) predicts a 70 dB CMRR limit, which is insufficient for high quality biopotential recordings using standard equipment [10].

Current methods to achieve a reduced capacitance, resulting in what is known as "ultra-high" input impedance, rely on microelectronic design techniques, obtaining application specific integrated circuits (e.g., [11]–[15]) with augmented impedance by guarding, bootstrapping, and neutralization techniques. Capacitance neutralization has been successfully implemented with discrete components [16], [17], but it requires adjustment and it is difficult to implement. Power supply bootstrapping guards the input of an operational amplifier (OA) by driving its power supplies with an ac potential equal to the input signal, as represented in Fig. 1. In this way, the ac potential applied across the input impedance is effectively zero and no current flows through it. This is equivalent to an input impedance of infinite magnitude. Bootstrapping was implemented using operational amplifiers by Kootsey and Johnson [18], and was further developed in work by Lányi and Hribik [19]–[21]. A disadvantage of bootstrapping is that it increases component count and circuit complexity. Using active electrodes already represents an increase in complexity because supply lines are needed in addition to the signal wire.

Increased wire stiffness and electrode weight make artifacts more prone to occur [22]. Artifacts are as challenging in modern mobile biopotential readout systems as EMI and a variety of relatively complex solutions have been proposed such as

Manuscript received July 10, 2017; revised October 31, 2017; accepted January 13, 2018. This work was supported in part by the La Plata National University (UNLP), Argentina, under Project PPID I-219, in part by the ANPCyT, Argentina, under Project PICT-2015/2257, and in part by the CONICET, Argentina, under Project PIP-112-2015-0100558. This paper was recommended by Associate Editor G. Wang. *(Corresponding author: Federico Nicolás Guerrero.)*

The authors are with the Instituto de Investigaciones en Electrónica, Control y Procesamiento de Señales LEICI (UNLP-CONICET), La Plata 1900, Argentina, and also with the National Scientific and Technical Research Council (CONICET), CCT La Plata B1904CMC, Argentina (e-mail: federico.guerrero@ing.unlp.edu.ar; spinelli@ing.unlp.edu.ar).

Color versions of one or more of the figures in this paper are available online at http://ieeexplore.ieee.org.

Digital Object Identifier 10.1109/TBCAS.2018.2796581

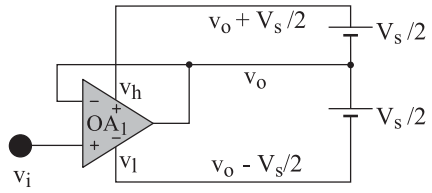

Fig. 1. Power supply bootstrapping allows an amplifier to present a high input impedance, useful for rejecting EMI in biopotential measurements with dry electrodes or improving measurements with patch-clamp electrode technique. This figure shows a conceptual circuit for a unity-gain buffer active electrode with power supply bootstrapping. Supply rails are fed a voltage equal to the input, dc shifted by V_s. Bootstrapping topologies increase circuit complexity.

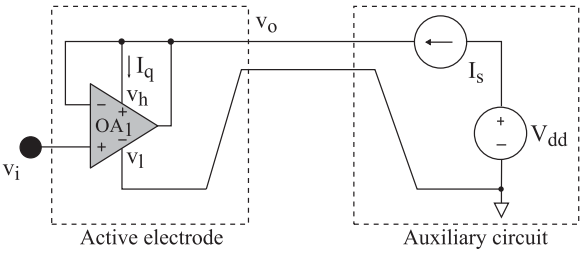

Fig. 2. Two-wired active electrodes can help alleviate artifacts increasing the leads compliance and simplifying the deployment of electrodes. This figure shows a remarkably simple two-wired active electrode design proposed by Degen *et al.* [9] using a single operational amplifier in unity gain buffer configuration. The input impedance of active electrodes implemented with low noise OAs is limited by the input capacitance of these devices.

impedance monitoring [23] or signal processing coupled with additional circuitry [24]. One approach to mitigate artifacts, complementary to other techniques, is the use of two-wired electrodes. These types of active electrodes share power and signal in one wire increasing the mechanical compliance of the leads or decreasing their cost, and simplifying the deployment of systems with a large number of electrodes. Commercial EEG active electrode acquisition systems such as ActiveTwo from Biosemi and g.SAHARA from g.tec successfully use this technique. Most published ultra-high impedance active electrodes have been implemented with a higher number of wires, from 3 to 6, as shown as part of a survey in [25].

Two-wired electrodes were thoroughly researched by Degen [26] who obtained simple and robust implementations. Degen *et al.* [9] compared two implementations: one based on a single transistor, well suited for ac coupled measurements, and another based on an operational amplifier (OA) suitable for dc coupled measurements. The OA-based implementation, which can be seen in Fig. 2, is composed of an unity gain buffer with its positive supply v_h also connected to the output node. A current source injects a constant current I_s into this node. I_s provides the quiescent supply current I_q and output current for the OA, while allowing the potential at node v_o to float freely. The output voltage is then

$$v_\mathrm{o} = \frac{(I_\mathrm{s} - I_\mathrm{q})\, R_\mathrm{o}}{A_\mathrm{ol} + 1} + v_\mathrm{i} \frac{A_\mathrm{ol}}{A_\mathrm{ol} + 1} \approx v_\mathrm{i} \qquad (2)$$

where A_ol is the open loop gain of the OA and the first term of the central member depends on approximately constant parameters. Hence, one wire with potential $v_\mathrm{o} \equiv v_\mathrm{h}$ follows the ac input

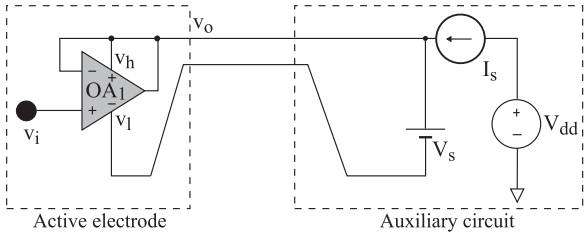

Fig. 3. Conceptual circuit for the proposed electrode using ideal components. OA_1 together with the passive electrode constitute the active electrode while the power supply bootstrapping circuit is placed on the main board of the acquisition system.

v_i while carrying the positive supply current. Therefore, no additional wire is needed to convey the biopotential signal.

Ultra-high input impedance active electrodes and two-wired topologies are two solutions for the most challenging problems faced by dry-electrode systems: EMI and artifacts. In this work we propose a novel circuit topology that combines the best aspects of both solutions by creating a power supply bootstrapping circuit using a two-wired topology. Hence, a high input impedance is obtained with a very simple circuit on the electrode using off-the-shelf components.

II. Method

The two-wired active electrode topology from Fig. 2 [9] forces the positive supply rail to follow the input voltage, therefore providing "half" a power supply bootstrap, since $v_\mathrm{h} = v_\mathrm{o} \approx v_\mathrm{i}$ as demonstrated by (2). This bootstrap reduces internal capacitance C_h, and the output signal can be used as an active guard to reduce parasitic impedance components. However, the input impedance of the electrode is limited by the internal capacitance to v_l, C_l.

A power supply bootstrap can be completed as shown in the conceptual schematic of Fig. 3, which allows to reduce C_l thus obtain a high-impedance active electrode. The proposed design forces the negative supply rail v_l to follow the potential v_i, with a dc shift V_s. V_s should be high enough to provide the necessary supply voltage for OA_1. The resulting circuit can be divided into a buffer presenting high input impedance and low output impedance (constituting the active electrode together with the contact plate), connected through only 2 wires with the auxiliary circuit on the main board of the acquisition system.

In the following subsections we first calculate the theoretical impedance improvement achieved by bootstrapping an OA in order to define important parameters needed to describe our solution. Next, we present an implementation of the proposed topology and finally we detail the experimental setups used to validate its functioning.

A. Input Impedance Analysis

The input impedance of an operational amplifier can be considered to be divided between an impedance Z_ih referred to the positive supply rail v_h and another Z_il referred to the negative supply rail v_l [19], as shown in Fig. 4. The relative contribution of Z_ih and Z_il to the total input impedance is not generally

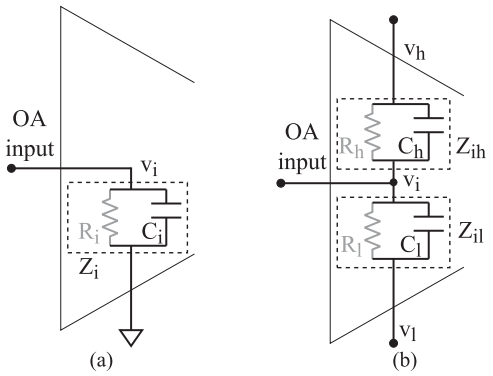

Fig. 4. Two models for the common-mode input impedance of an operational amplifier (either inverting or non-inverting inputs). (a) The total contribution of all impedances to ground is represented by the equivalent impedance Z_i. (b) A more detailed model [19], where impedances Z_{il} and Z_{ih} to the v_h and v_l supply terminals are included. Differential impedance was disregarded because the OA is expected to operate under negative feedback.

specified for commercial components. Instead, the total common mode impedance is given.

The proposed circuit of Fig. 3 ideally produces potentials v_h and v_l with ac components equal to those of v_i in order to reduce currents through $Z_{l,h}$. However, the practical implementations of the positive and negative bootstrapping circuits will have transferences close but not equal to 1, such that

$$v_\mathrm{h} = v_\mathrm{i}\,\alpha_\mathrm{h}(s) \tag{3}$$

$$v_\mathrm{l} = v_\mathrm{i}\,\alpha_\mathrm{l}(s) - V_\mathrm{s} \tag{4}$$

with α_h(s) and α_l(s) ≈ 1 up to a given frequency. The input current thus results

$$i_\mathrm{i} = \frac{v_\mathrm{i} - v_\mathrm{i}\alpha_h}{Z_{ih}} + \frac{v_\mathrm{i} - (v_\mathrm{i}\alpha_l - V_\mathrm{s})}{Z_{il}}\ , \tag{5}$$

yielding an ac input current equal to:

$$i_{\mathrm{i,ac}} = v_\mathrm{i}\left(\frac{1-\alpha_h}{Z_{ih}} + \frac{1-\alpha_l}{Z_{il}}\right). \tag{6}$$

At this point, it is best to simplify (6) by defining a factor $\gamma(s) = 1/(1-\alpha(s))$. Because α is close to 1, γ will be a high-valued gain, hence γ will be referred to as "bootstrap gain".

Thus, the impedance seen from the input node can be obtained from (6) as:

$$\frac{v_\mathrm{i}}{i_\mathrm{i}} = \left(\frac{1}{Z_{ih}\gamma_h} + \frac{1}{Z_{il}\gamma_l}\right)^{-1}. \tag{7}$$

The total impedance is the parallel of impedances between the input node and each supply node, augmented by their corresponding bootstrap gain.

Disregarding the resistive component of the input impedance, as depicted in Fig. 4(b), $Z_{il,ih}$ can be represented by $C_{l,h}$ and as a consequence the effective impedance with bootstrapping results in a parallel of values C_h/γ_h and C_l/γ_l where the contribution of C_h and C_l to the total capacitance is generally not known.

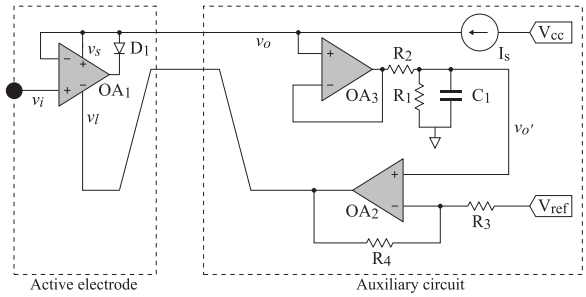

Fig. 5. Practical implementation of the proposed topology. OA_1 and D_1 can be placed on a small board together with the electrode, conforming a minimal part-count active electrode, connected with two wires to the main board where the auxiliary circuit is placed. The power supply for OA_2 and OA_3 is provided on the main board where V_cc and ground are available.

B. Circuit Design

A practical implementation of the design can be seen in Fig. 5, where ideal blocks have been replaced with practical counterparts suitable for implementation.

A summing amplifier, implemented using OA_2, produces the desired dc shift. Its output is:

$$v_\mathrm{l} = v'_\mathrm{o}\left(1 + \frac{R_4}{R_3}\right) - V_\mathrm{ref}\frac{R_4}{R_3}. \tag{8}$$

For convenience the factor $(1 + R_4/R_3)$ will be named G_1 obtaining

$$v_\mathrm{l} = v'_\mathrm{o}G_1 - V_\mathrm{ref}\,(G_1 - 1)\,. \tag{9}$$

The bootstrap needs v_l to be equal to v_i, which can be achieved using the potential divider formed by R_1 and R_2. The relation between v'_o and v_o is:

$$v'_\mathrm{o} = v_\mathrm{o}\frac{R_1}{R_1+R_2}\frac{1}{1+\mathrm{sC_1R_1||R_2}} = v_\mathrm{o}G_2. \tag{10}$$

Substituting v'_o in (9) with (10) yields the following expression for v_l:

$$v_\mathrm{l} = v_\mathrm{o}G_2G_1 - V_\mathrm{ref}\,(G_1 - 1)\,,$$

where $G_1 \times G_2$ determines the proportionality constant of the negative source bootstrap and will therefore be named α_l, and the obtained dc shift should be equal to V_s so that:

$$v_\mathrm{l} = v_\mathrm{o}\alpha_\mathrm{l} - V_\mathrm{s}.$$

Therefore:

$$\alpha_\mathrm{l} = \frac{1+R_4/R_3}{1+R_2/R_1}\,(1+\mathrm{sC_1R_1||R_2})^{-1} \tag{11}$$

$$V_\mathrm{s} = V_\mathrm{ref}\,(G_1 - 1)\,. \tag{12}$$

Given the desired dc shift V_s, G_1 can be set using R_3 and R_4 to fulfill (12). This is convenient because V_ref can be obtained from a single low-noise reference voltage shared by many electrodes. Next, G_2 can be set using R_1 and R_2 to achieve a target low frequency value for α_l according to the gain of (11). The capacitor C_1 degrades the bootstrap at higher frequencies in order to ensure stability. Once R_1 and R_2 are set, the time constant of

(11) can be set to a value one decade below the gain-bandwidth product of OA_1.

OA_2 performs the desired dc shift and also acts as voltage source allowing to impose the v_l potential necessary for the negative rail bootstrap, while sinking current I_s. OA_3 buffers v_o to avoid loading OA_1 with the impedance of $R_{1,2}$ and C_1. This topology decouples the negative bootstrap circuit from the output of the electrode, hence (2) holds.

It must be noted that replacing V_s in (5) using (12) shows that ac perturbations in V_ref have an effect on the input current causing a voltage drop on the impedance of the electrode. The bootstrap will not reduce this effect. Thus, V_ref should be implemented with a low noise, well regulated source.

C. Operational Amplifier Requirements

Operational amplifier OA_1 must be a rail-to-rail input/output device (known as "RRIO" in the technical literature). The input of a RRIO OA can usually reach the potential of the supply rails. However, when the output voltage is close to the supply rails, the output current increases considerably. Thus, as presented in a two-wired amplifier implementation by Degen and Jäckel [27], diode D_1 is included to push the output voltage away from the positive rail. The inclusion of D_1 allows I_s to be programmed with a smaller current, lowering power consumption.

The presented topology needs in particular OAs that allow the input to be taken a few mV *above* the positive supply rail. This is not a restrictive requirement, as many RRIO OAs fulfill it.

The open loop gain of OA_1 becomes specifically relevant in this design because it affects the power supply rejection of the circuit. The first term of (2) shows that variations in I_s can affect the output. I_s can vary due to fluctuations in V_dd, which is the power supply of the complete circuit, through a factor δ_I. Applying superposition and manipulating (2), PSRR_+ results:

$$\mathrm{PSRR}_+ \approx \frac{A_\mathrm{ol}}{\delta_\mathrm{I} R_\mathrm{o}}. \tag{13}$$

The coefficient δ_I is usually better than 0.1%/V (for a well-known commercial device as LM334, it is typically 0.02%/V) while R_o is usually at or below the order of 1 kΩ, hence a pessimistic assumption is $\mathrm{PSRR}_+ \approx A_\mathrm{ol}$.

Finally, some electrostatic-discharge (ESD) protection circuits can short-circuit the input at start-up. Although the design of the input stage is generally not know, devices labeled as having "limited ESD protection" should be used.

D. Circuit Implementation

The circuit from Fig. 5 was built using OPA333 which satisfies all requirements to implement OA_1: it is RRIO, has limited ESD protection, a minimum operating voltage of 1.8 V, and low voltage and current noise. It also has a small package which is convenient to implement active electrodes reduced in size and weight. A surface mount 1N4148 diode was used for D_1 and both components were mounted on a 15×20 mm printed circuit board (PCB) with two connectors for the two-wired lead, as seen in Fig. 6.

Fig. 6. Photograph of the implemented active electrode with two-wire leads. The inset shows the PCB layout and component placement.

The bootstrapping circuit was implemented on a bigger board placed on the main acquisition system box which had a 5 V power supply. OA_2 and OA_3 were implemented using a dual OA OPA2320. The current source I_s was implemented with a LM334 which has a minimum compliance of 1.1 V. This voltage sets the maximum positive excursion of the active electrode; its output cannot attain a value higher than the total supply voltage minus the current source compliance. In this case, $5\,\mathrm{V} - 1.1\,\mathrm{V} = 3.9\,\mathrm{V}$. The LM334 was programmed with 0.9 mA, enough to obtain approximately 0.65 V across D_1 with a low dynamic resistance below 10 Ω, while providing the tens of μA needed for OPA333's I_q.

A 3.5 V V_ref was selected for the system allowing a positive excursion of $3.9\,\mathrm{V} - 3.5\,\mathrm{V} = 400\,\mathrm{mV}$. A 2.5 V supply voltage V_s was selected for OA_1, thus allowing a negative excursion of $3.5\,\mathrm{V} - 2.5\,\mathrm{V} = 1\,\mathrm{V}$.

Having configured v_s and V_ref, $R_3 = 4.7\,\mathrm{k\Omega}$ and $R_4 = 3.3\,\mathrm{k\Omega}$ were used so $V_\mathrm{s} = 2.46\,\mathrm{V}$ was obtained and finally $R_1 = 1\,\mathrm{k\Omega}$ and $R_2 = 720\,\Omega$ were selected to produce a dc magnitude for $\alpha_\mathrm{l} \approx 0.98$. The value of α_l was chosen as a first coarse approximation to ensure a bootstrap gain γ_l that would reduce the 4 pF input capacitance of the OPA333 (reported in its datasheet) below a target 100 fF, considering the effect of the negative rail bootstrap as the dominant term in (7).

The active electrode seen in Fig. 6 was encapsulated in a plastic cover lined with conductive copper tape connected to the buffer output. The cover acted as a guard for the sensitive input node in order to avoid parasitic capacitances that could degrade the input impedance. The small enclosure also acted as shielding to avoid capacitively coupled EMI.

E. Measurement Setup

Acquisition system: An acquisition system described in a previous publication by the authors [28] was used. It is based around the ADS1299 front-end from Texas Instruments with 8 differential measurement channels. The system has an independent body potential driving circuit with its own common mode measurement and feedback electrodes that allow imposing the desired dc potential on the body (set to 3.5 V as needed by the electrodes). The system provides an isolated 5 V supply to power the active electrodes and admits both single ended and differential inputs.

Two further pairs of electrodes were built using OPA333 OAs in order to conduct comparative measurements. One pair

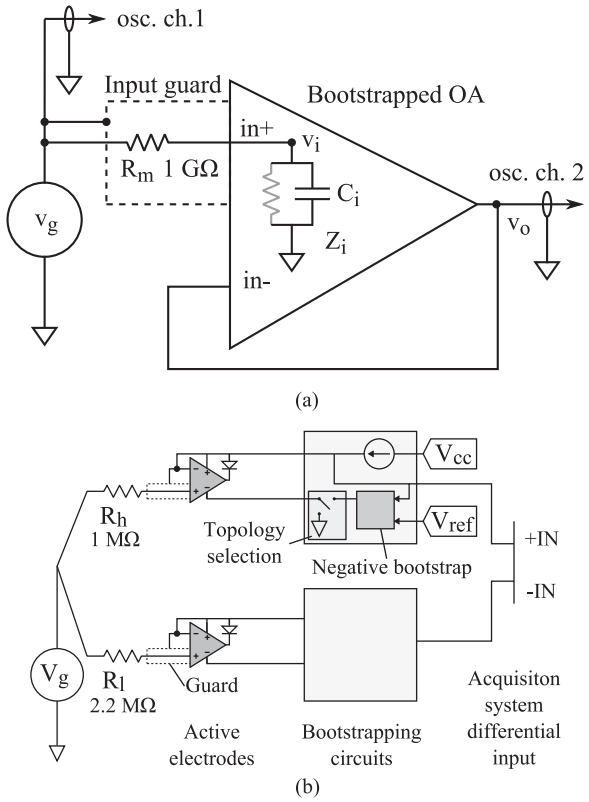

Fig. 7. Measurement circuits. (a) Input impedance measurement setup. (b) Measurement of CMRR limit due to the potential divider effect.

was configured as a traditional active electrode with unity gain feedback and 3 wires, the second was configured as a two-wired buffer from Fig. 2.

Input impedance: In order to measure the input impedance, a simple potential divider was formed as depicted in Fig. 7(a). A 1 GΩ resistor R_{m} was placed as source impedance, a sine wave frequency sweep was applied and the input-output relative phase $\Delta\phi$ was measured. The resistive component of the input impedance was neglected so the input capacitance was estimated as $C_{\mathrm{i}} = \tan^{-1}(\Delta\phi)/(2\pi f_{\mathrm{g}} R_{\mathrm{m}})$. The same measurement was conducted for the traditional 3-wired buffer, the 2-wired buffer, and the proposed electrode.

All electrodes were mounted on PCBs with similar layout and active shielding was used to avoid stray couplings to external potentials. The output of the buffers was routed surrounding the input pin and adhesive copper tape was used, also connected as active shield, above and below OA_1.

Common mode rejection improvement: The improvement in common mode interference rejection due to the reduced potential divider effect was experimentally tested with a 1.2 MΩ impedance unbalance.

Common mode signals were applied to a differential channel through an unbalanced source impedance formed by a 2.2 MΩ and a 1 MΩ resistor, as shown in Fig. 7(b). The common mode signals were 100 mV amplitude sine waves applied using a function generator referred to the system's 3.5 V reference voltage. A frequency sweep from 10 Hz to 1000 Hz was conducted for each pair of buffers connected to the acquisition system. The high resolution of the system (that relies on 24 bit analog-to-digital converters) allowed to measure very small CM signals, therefore making it unnecessary to use a high valued impedance as in the previous experiment and allowing testing under a realistic condition of 1 MΩ unbalance.

TABLE I
MEASURED INPUT CAPACITANCE

Configuration	Total common mode input capacitance [pF]
Buffer electrode	5.18
Two-wired electrode	3.47
Proposed electrode	0.071

The circuits were fully shielded for this experiment as described in the previous section.

Biopotential measurements: Biopotential measurements were carried out using the described acquisition system and the implemented active electrodes. Circular stainless steel contact plates with a 10 mm diameter were used for ECG measurements, whereas a finger-type dry electrode was used for EEG measurements. Elastic fabric bands were used to affix the electrodes to the body in all locations.

III. RESULTS AND DISCUSSION

A. Input Impedance and CMRR Improvement

The input impedance of the proposed electrode resulted in C_i =71 fF, measured as described in Section II-E between 10 Hz to 900 Hz and with a standard deviation across measurements of 4 fF. The proposed method was successful in reducing the input capacitance almost two orders of magnitude compared with a traditional buffer.

Table I shows the measured capacitance for the three types of electrodes implemented with the same operational amplifier. These values allow determining the impedance boosting provided by the two-wired topology by itself, thanks to its "half bootstrap", and the contribution of the proposed topology. At the same time, the values of the unknown capacitances C_{h} and C_{l} can be estimated.

The two-wired electrode from Fig. 2 reduced the total capacitance from 5.18 pF to 3.47 pF. Assuming that C_{l} remained constant, and considering that the high-side bootstrap of this topology is very good (since v_{h} is directly connected to v_{o}), then this total capacitance reduction is due to the annulling of C_{h}. Hence, $C_{\mathrm{h}} = 1.71$ pF.

The partial v_{h} bootstrap of the two-wired electrode is hence responsible for completely reducing C_{h}, however it still has a 3.47 pF input capacitance. This capacitance is therefore given by C_{l}, coupled to the negative supply node v_{l}. The two-wired electrode from Fig. 2 achieves an impedance boost of approximately 1.49 times.

The proposed electrode further diminishes the input capacitance by reducing C_{l} through the negative rail bootstrapping to 0.071 pF. This implies a negative bootstrap gain $\gamma_{\mathrm{l}} = 48$, which closely matches the designed $\alpha_{\mathrm{l}} = 0.98$ that would yield a factor $\gamma_{\mathrm{l}} = 49.9$.

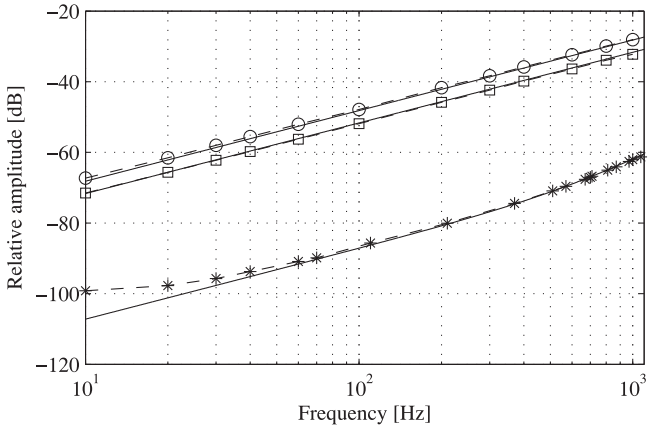

Fig. 8. Comparison of CM to DM transformation due to a 1.2 MΩ input impedance unbalance using standard 3 wire buffer active electrodes (circle markers), 2-wired electrodes (square markers), and the proposed electrode (asterisk markers). Theoretical curves, in full line, are superposed to experimental results. A deviance is noticed on lower frequencies due to the CMRR limit of the acquisition system.

Distinguishing capacitances $C_{\rm h}$ and $C_{\rm l}$ allows predicting the improvement regarding the potential divider effect. When the traditional 3-wired electrode is used (1) depends on the combination of $C_{\rm h} + C_{\rm l} = C_{\rm in}$ and hence the CM to input DM gain due to source impedance unbalance is:

$$G_{\rm CD,3w} = \Delta R_{\rm s} 2\pi f \; C_{\rm in}. \tag{14}$$

The case of the 2-wired electrode is similar, but $C_{\rm h}$ can be considered equal to 0 and the rejection is:

$$G_{\rm CD,2w} = \Delta R_{\rm s} 2\pi f \; C_{\rm l}. \tag{15}$$

Finally, the proposed electrode further reduces $C_{\rm l}$ with a frequency dependent transfer function given by $\gamma_l(s)$, obtained from 11, thus

$$G_{\rm CD,b2w} = \Delta R_{\rm s} 2\pi f \; C_{\rm l}\gamma_l(s). \tag{16}$$

The curves given by (14)–(16) were graphed in Fig. 8 in full black line. In the same figure, the results from the CMRR measurements conducted with a 1.2 MΩ unbalance for the 3 types of electrodes are also shown. The theoretical and experimental curves showed a good match, demonstrating the correct operation of the bootstrapping circuit. A MSE fitting of linear curves produced capacitance values with a match closer than 5% to the measured ones.

The proposed circuit provided a 34 dB improvement in CMRR for the fundamental power-line frequency and its harmonics up to 400 Hz. The resulting CMRR at 50 Hz was approximately 92 dB. The experimental and theoretical curves show a difference in the lower frequency range due to the CMRR limit of the measurement system, as the total CMRR of cascaded stages with unity gain is [29]

$$\mathrm{CMRR}_{\rm total} = \left(\sum \mathrm{CMRR}^{-1}_{\rm stage\ i}\right)^{-1}. \tag{17}$$

The measured CMRR of the acquisition system including the proposed electrodes was 103.5 dB between 1 and 250 Hz.

TABLE II
NOISE VALUES FOR THE PROPOSED ELECTRODE AND COMPARISON WITH THE ALTERNATIVES

Active electrode	Spectral amplitude* (average 10–100 Hz)	Total noise	
		EEG bandwidth (0.1–70 Hz)	EMG bandwidth (10–450 Hz)
	$\mathrm{nV}/\sqrt{\mathrm{Hz}}$	$\mu\mathrm{V_{rms}}$	$\mu\mathrm{V_{rms}}$
Proposed	79(3)	0.57	1.30
Two-wired	77(3)	0.55	1.25
Buffer	61(3)	0.46	1.08

*Numbers in parentheses represent standard deviation across measurements.

B. Noise Measurement

The noise of the electrode, as well as the noise corresponding to the alternative implementations using the same operational amplifier, is presented in Table II. The spectral amplitude was estimated using Welch's method, while the integrated noise was calculated using the standard deviation of the bandpass filtered signal using order 2 Butterworth filters with the bandwidths given in the table. The total noise is acceptable for biopotential measurements, being very well suited for EEG acquisition due to the lack of 1/f noise that the OPA333 presents. Low frequency noise, verified down to 0.01 Hz , also corresponded with the OPA333 characteristics.

Because the buffer amplifier ($\mathrm{OA_1}$) establishes a closed loop control of the output, assuming a linear feedback model the noise contribution from the auxiliary bootstrapping circuit is rejected by the open loop gain of $\mathrm{OA_1}$. Referring to Table II, results show that the noise of the proposed electrode was slightly higher than the equivalent buffer electrode, but virtually equal to the well-established two wired implementation from Fig. 2, which suggests that the contribution to the total noise from sources in the negative bootstrapping circuit (dominated by $\mathrm{OA_{2,3}}$ and $V_{\rm ref}$) is negligible.

C. Biopotential Measurements

ECG measurements were first conducted to validate the buffer as active electrode against a well-established alternative. Therefore the proposed electrodes were placed on the right and left arms of a volunteer and simultaneously traditional 3-wired electrodes were placed 1 cm apart. The obtained recordings can be seen in Fig. 9 band-pass filtered with a 2nd order Butterworth filter from 0.05 Hz to 150 Hz. The direct subtraction of both recordings is displayed on the lower trace. A 10 s difference signal from the same recordings, bandpass filtered between 0.1 Hz to 100 Hz, had a 71 $\mu\mathrm{V_{pp}}$ noise which is below the required resolution for clinical ECG of ± 40 μV [30].

Next, EEG measurements were conducted using dry, finger-type electrodes to test the buffer performance in a low noise, challenging dry-contact measurement application. One electrode was placed near $\mathrm{F_{p1}}$ position and the other on the $\mathrm{O_2}$ position, wiggling it lightly through hair so some of its fingers (implemented with 0.64×3 mm gold plated rods) made contact with the scalp. The DRL was placed on the forehead near F_{pz} and several recordings were made while alpha rhythms were

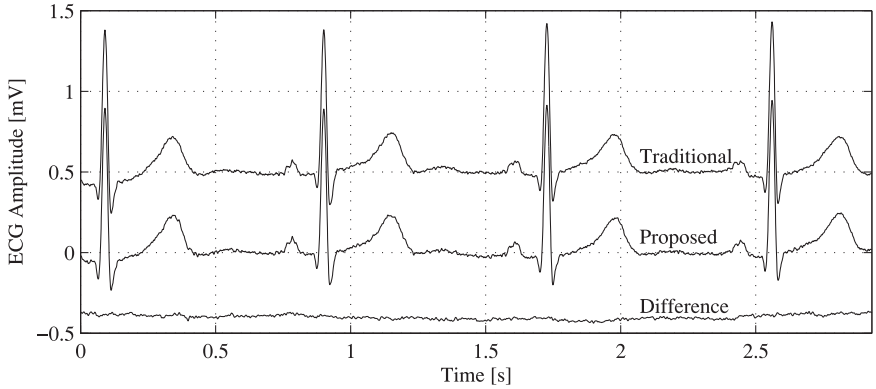

Fig. 9. ECG signals acquired simultaneously with the traditional 3 wire buffer active electrode (upper trace) and the proposed electrode, placed 1 cm apart from each other, from the arms of a volunteer. The subtraction between the two signals is shown in the lower trace. DC-shifts between the signals were introduced for display convenience.

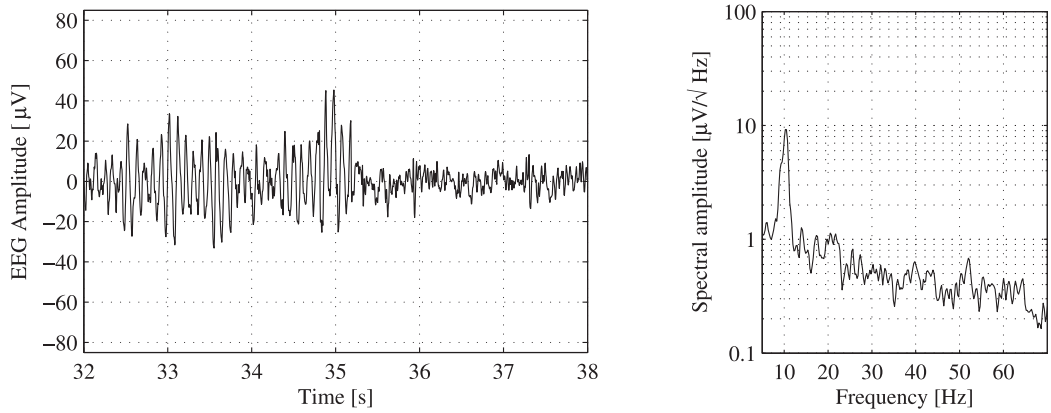

Fig. 10. (a) EEG signal presenting an alpha rhythm, captured using dry finger-type EEG active electrodes implemented with the proposed circuit. The baseline noise can be seen when the eyes of the subject were opened and the rhythm faded. (b) Amplitude spectrum of an acquired 10 s alpha rhythm signal.

elicited by visual relaxation. A sample of the obtained signal can be seen in Fig. 10(a) next to the amplitude spectrum of a 10 s recording with sustained presence of an alpha rhythm in Fig. 10(b).

D. Parameter Discussion

The functioning parameters of the proposed active electrode are summarized in Table III, where a selection of parameters from other biopotential readout systems from the literature has also been displayed for comparison. Further comparative figures can be found in a recent review by Xu *et al.* [25]. The achieved CMRR improvement is comparable with that achieved by Zhou *et al.* that maintain a 78 dB CMRR with a 1 MΩ unbalance [32]. At the same time, the 71 fF input capacitance is in the order of those in the literature (60 fF [11], 45 fF [31]). Recently, designs surpassing this order of magnitude and intended for biopotential measurements were presented by Joshi *et al.* [33] achieving a 7 fF capacity and Zhou [15], however these devices were not yet experimentally tested in biopotential measurements.

The linear range of the circuit extends form 2.5 V to 3.9 V allowing a 1.4 V single-ended excursion. If a lower input range is tolerated, the supply voltage of the system could be lowered as long as the minimum voltage supply for OA_1 and I_s compliance are guaranteed (as would be the case with OPA333 1.8 V operation and LM334 1.1 V compliance, allowing a 400 mV single-ended range for a 3.3 V system).

The presented active electrode is positioned within or above the parameter range of previously developed alternatives according to the pursued objectives: a 2-wired, dc-coupled, active electrode implementation achieving ultra-high input impedance on par with state-of-the-art implementations, using commercial off-the-shelf components available to a broad set of designers.

Recent work from Fang *et al.* [34] implements a similar concept allowing to provide active shielding to a two-wired active electrode based on a single transistor that implements a capacitive electrode. The transistor-based approach is suitable for ac-coupled measurements, but not for dc-coupled measurements [9].

The main drawback of the presented implementation is power consumption which is in the mA range due to the polarization of D_1 and the high energy consumption of the OPA2320 OA. This is not nevertheless a fundamental limitation of the conceptual design and may be addressed by technical improvements such as using lower consumption OAs for the auxiliary circuit (potential candidates could be TLV2432 or OPA2333 dual OAs) and exploring the use of a micro-power voltage references in place of D_1 (such as LT1004).

TABLE III
PARAMETER COMPARISON WITH HIGH INPUT-IMPEDANCE BIOPOTENTIAL READOUT SYSTEMS

Key	Degen 06 [27]	Chi 11 [11]	Nasserian 16 [31]	Zhou 16 [32]	This work
Input impedance	1 TΩ @ DC	60 fF	45 fF	6.7 GΩ @ 50 Hz	71 fF
Wires	2	4	3*	3*	2
Noise	7.4 μV_{rms} 1 Hz to 1000 Hz	45 $nV/\sqrt{Hz}$ at 1 kHz	2.62 μV_{rms} 0.5 Hz to 100 Hz	0.67 μV_{rms} 0.5 Hz to 100 Hz	0.57 μV_{rms} 0.1 Hz to 70 Hz
CMRR	78 dB	82 dB	110 dB	86 dB 78 dB–1 MΩ†	103 dB 92 dB–1.2 MΩ†
Coupling	DC	DC	AC	DC suppression	DC
Voltage Gain	100	3–100	1000	1 (AE)	1
Supply	5 V 7.5 mW	3.3 V 1.5 μA	±0.5 V 200 nW	1.8 V 60 μA	5 V 25 mW
Electrode offset tolerance‡	±250 mV	>±1 V	–	±200 mV	±1.4 V
Implementation	Discrete	ASIC	Simulated ASIC	ASIC	Discrete

*Not Mentioned in the publications. It can be inferred that at least 3 wires were necessary.
† CMRR at 50 Hz when including the specified impedance unbalance in the differential channel.
‡ Considering a differential pair of electrodes. A single AE input would achieve half this range.
Categories based on similar comparisons as seen in a review by Xu *et al.* [25] and in work by Zhou *et al.* [32].

IV. CONCLUSION

An active electrode circuit with ultra-high input impedance and two-wired leads was proposed. The input impedance was augmented through power supply bootstrapping with a topology that also allowed powering the electrode and delivering the measured signal using only two wires.

A prototype was implemented reducing the input capacitance of a 4 pF operational amplifier to 71 fF with a very low part-count circuit. The achieved capacitance reduction allowed a significant improvement in common mode to differential mode transformation due to source impedance unbalance, experimentally demonstrated for a 1.2 MΩ unbalance achieving a 34 dB improvement at power line frequency and boosting harmonic rejection up to 1 kHz. The proposed technique achieved these parameters using commercial, off-the-shelf components hence allowing its implementation by a broad set of users.

A set of requirements for the operational amplifiers that may be used in the design was given. The OA acting as a buffer needs to be a rail-to-rail input-output amplifier, to include a positive input excursion able to surpass the positive supply rail, its open loop gain must be high enough to guarantee the necessary power supply rejection ratio, and finally the OA needs to have *limited* electrostatic discharge protection.

The circuit was validated as a biopotential measurement active electrode, showing a performance equal to the established 3-wired buffer alternative in ECG measurements and demonstrating the feasibility of EEG measurements using dry electrodes.

REFERENCES

[1] L. Geddes and M. Valentinuzzi, "Temporal changes in electrode impedance while recording the electrocardiogram with "dry" electrodes," *Ann. Biomed. Eng.*, vol. 1, no. 3, pp. 356–367, 1973.
[2] A. Searle and L. Kirkup, "A direct comparison of wet, dry and insulating bioelectric recording electrodes," *Physiol. Meas.*, vol. 21, no. 2, pp. 271–283, 2000.
[3] N. Gandhi, C. Khe, D. Chung, Y. M. Chi, and G. Cauwenberghs, "Properties of dry and non-contact electrodes for wearable physiological sensors," in *Proc. 2011 Int. Conf. Body Sensor Networks*, 2011, pp. 107–112.
[4] H. C. Jung *et al.*, "CNT/PDMS composite flexible dry electrodes for long-term ECG monitoring," *IEEE Trans. Biomed. Eng.*, vol. 59, no. 5, pp. 1472–1479, May 2012.
[5] B. Taji, S. Shirmohammadi, V. Groza, and I. Batkin, "Impact of skin-electrode interface on electrocardiogram measurements using conductive textile electrodes," *IEEE Trans. Instrum. Meas.*, vol. 63, no. 6, pp. 1–11, Jun. 2014.
[6] M. Yokus and J. Jur, "Fabric-based wearable dry electrodes for body surface biopotential recording," *IEEE Trans. Biomed. Eng.*, vol. 63, no. 2, pp. 423–430, Feb. 2016.
[7] S. L. Kappel and P. Kidmose, "Study of impedance spectra for dry and wet earEEG electrodes," in *Proc. 37th Annu. Int. Conf. IEEE Eng. Med. Biol. Soc.*, Aug. 2015, pp. 3161–3164.
[8] J. C. Huhta and J. G. Webster, "60-Hz interference in electrocardiography," *IEEE Trans. Biomed. Eng.*, vol. BME-20, no. 2, pp. 91–101, Mar. 1973.
[9] T. Degen, S. Torrent, and H. Jäckel, "Low-noise two-wired buffer electrodes for bioelectric amplifiers," *IEEE Trans. Biomed. Eng.*, vol. 54, no. 7, pp. 1328–32, Jul. 2007.
[10] A. C. Metting van Rijn, A. Peper, and C. A. Grimbergen, "High-quality recording of bioelectric events. Part 1. Interference reduction, theory and practice," *Med. Biol. Eng. Comput.*, vol. 28, no. 5, pp. 389–397, 1990.
[11] Y. M. Chi, C. Maier, and G. Cauwenberghs, "Ultra-high input impedance, low noise integrated amplifier for noncontact biopotential sensing," *IEEE J. Emerg. Sel. Topics Circuits Syst.*, vol. 1, no. 4, pp. 526–535, Dec. 2011.
[12] J. Xu, R. F. Yazicioglu, B. Grundlehner, P. Harpe, K. A. A. Makinwa, and C. Van Hoof, "A 160 μW 8-channel active electrode system for EEG monitoring," *IEEE Trans. Biomed. Circuits Syst.*, vol. 5, no. 6, pp. 555–567, Dec. 2011.
[13] M. Guermandi, R. Cardu, E. F. Scarselli, and R. Guerrieri, "Active electrode IC for EEG and electrical impedance tomography with continuous monitoring of contact impedance," *IEEE Trans. Biomed. Circuits Syst.*, vol. 9, no. 1, pp. 21–33, Feb. 2015.
[14] K. A. Ng and Y. P. Xu, "A compact, low input capacitance neural recording amplifier," *IEEE Trans. Biomed. Circuits Syst.*, vol. 7, no. 5, pp. 610–620, Oct. 2013.
[15] Z. Zhou and P. A. Warr, "A high input impedance low noise integrated front-end amplifier for neural monitoring," *IEEE Trans. Biomed. Circuits Syst.*, vol. 10, no. 6, pp. 1079–1086, Dec. 2016.
[16] D. Dobrev, T. Neycheva, and N. Mudrov, "Simple two-electrode biosignal amplifier," *Med. Biol. Eng. Comput.*, vol. 43, no. 6, pp. 725–30, 2005.
[17] E. Spinelli and M. Haberman, "Insulating electrodes: A review on biopotential front ends for dielectric skin-electrode interfaces," *Physiol. Meas.*, vol. 31, no. 10, p. S183–S198, Oct. 2010.
[18] J. M. Kootsey and E. A. Johnson, "Buffer amplifier with femtofarad input capacity using operational amplifiers," *IEEE Trans. Biomed. Eng.*, vol. 20, no. 5, pp. 389–391, Sep. 1973.
[19] S. Lányi, "The noise of input stages with low parasitic capacitance," *Meas. Sci. Technol.*, vol. 12, no. 9, pp. 1456–1464, 2001.
[20] S. Lányi and M. Pisani, "A high-input-impedance buffer," *IEEE Trans. Circuits Syst. I, Fundam. Theory Appl.*, vol. 49, no. 8, pp. 1209–1211, Aug. 2002.

[21] J. Hribik, S. Lányi, and M. Hruskovic, "A high-input-impedance buffer," in *Proc. 18th Int. Conf. Radioelektronika*, 2008, pp. 1–4.
[22] S. Roy, G. De Luca, M. Cheng, A. Johansson, L. Gilmore, and C. De Luca, " Electro-mechanical stability of surface EMG sensors," *Med. Biol. Eng. Comput.*, vol. 45, no. 5, pp. 447–457, May 2007.
[23] N. Van Helleputte, S. Kim, H. Kim, J. P. Kim, C. Van Hoof, and R. F. Yazicioglu, "A 160 μA biopotential acquisition IC with fully integrated IA and motion artifact suppression," *IEEE Trans. Biomed. Circuits Syst.*, vol. 6, no. 6, pp. 552–561, Dec. 2012.
[24] T. Niederhauser *et al.*, "A baseline wander tracking system for artifact rejection in long-term electrocardiography," *IEEE Trans. Biomed. Circuits Syst.*, vol. 10, no. 1, pp. 255–265, Feb. 2016.
[25] J. Xu, S. Mitra, C. Van Hoof, R. Yazicioglu, and K. A. A. Makinwa, "Active electrodes for wearable EEG acquisition: Review and electronics design methodology," *IEEE Rev. Biomed. Eng.*, vol. 10, pp. 187–198, 2017.
[26] T. W. Degen, "Portable devices for mobile health monitoring," Ph.D. dissertation, ETH Zurich, Université de Neuchâtel, 2011.
[27] T. Degen and H. Jäckel, "A pseudodifferential amplifier for bioelectric events with dc-offset compensation using two-wired amplifying electrodes," *IEEE Trans. Biomed. Eng.*, vol. 53, no. 2, pp. 300–310, Feb. 2006.
[28] F. N. Guerrero and E. Spinelli, "High gain driven right leg circuit for dry electrode systems," *Med. Eng. Phys.*, vol. 39, pp. 117–122, 2017.
[29] R. Pallas-Areny and J. Webster, "Common mode rejection ratio in differential amplifiers," *IEEE Trans. Instrum. Meas.*, vol. 40, no. 4, pp. 669–676, Aug. 1991.
[30] *Diagnostic Electrocardiographic Devices*, ANSI/AAMI Std. EC11, Rev. 2007, 1991.
[31] M. Nasserian, A. Peiravi, and F. Moradi, "A 1.62 μW 8-channel ultra-high input impedance EEG amplifier for dry and non-contact biopotential recording applications," in *Proc. 2016 IFIP/IEEE Int. Conf. Very Large Scale Integr.*, Sep. 2016, pp. 1–6.
[32] X. Zhou, Q. Li, S. Kilsgaard, F. Moradi, S. L. Kappel, and P. Kidmose, "A wearable ear-EEG recording system based on dry-contact active electrodes," in *Proc. 2016 IEEE Symp. VLSI Circuits*, Jun. 2016, pp. 1–2.
[33] S. Joshi, C. Kim, and G. Cauwenberghs, "A 6.5-μW/MHz charge buffer with 7-fF Input capacitance in 65-nm CMOS for noncontact electropotential sensing," *IEEE Trans. Circuits Syst. II, Exp. Briefs*, vol. 63, no. 12, pp. 1161–1165, Dec. 2016.
[34] H. Fang *et al.*, "Capacitively coupled arrays of multiplexed flexible silicon transistors for long-term cardiac electrophysiology," *Nat. Biomed. Eng.*, vol. 1, no. 4, 2017, Art. no. 0055.

Federico Nicolás Guerrero was born in Comodoro Rivadavia, Argentina, in 1986. He received the Engineering degree in electronics in 2011 and the Ph.D. degree in 2017 from La Plata National University (UNLP), La Plata, Argentina. Since 2012, he has been with the Instituto de Investigaciones en Electrónica, Control y Procesamiento de Señales LEICI (UNLP-CONICET), La Plata, Argentina, where he currently holds a postdoctoral fellowship from the National Scientific and Technical Research Council (CONICET), Argentina. He is also a Teaching Assistant with the UNLP Engineering Faculty. His research interests include instrumentation and control for biopotential measurement systems.

Enrique Mario Spinelli was born in Balcarce, Argentina, in 1964. He received the Engineer degree in electronics and the M.S. and Ph.D. degrees from La Plata National University (UNLP), La Plata, Argentina, in 1989, 2000, and 2005, respectively. Since 1990, he has been with the Instituto de Investigaciones en Electrónica, Control y Procesamiento de Señales LEICI (UNLP-CONICET) working on scientific instrumentation. He is currently a Professor in control systems with the Engineering Faculty, UNLP, and a Researcher with the National Scientific and Technical Research Council (CONICET), Argentina. His research interests include analog signal processing and brain control interfaces.